

We are IntechOpen, the world's leading publisher of Open Access books Built by scientists, for scientists

6,900

Open access books available

186,000

International authors and editors

200M

Downloads

Our authors are among the

154

Countries delivered to

TOP 1%

most cited scientists

12.2%

Contributors from top 500 universities



WEB OF SCIENCE™

Selection of our books indexed in the Book Citation Index
in Web of Science™ Core Collection (BKCI)

Interested in publishing with us?
Contact book.department@intechopen.com

Numbers displayed above are based on latest data collected.
For more information visit www.intechopen.com



Characterization of Complex Industrial Surfaces with Specific Structured Patterns

Yannick Caulier

Fraunhofer Institute for Integrated Circuits IIS, Erlangen, Germany

1. Introduction

Recent researches have demonstrated the importance of structured light patterns for use in the quality control of industrial workpieces. These researches have been focused on the adaptation of the projected light patterns and the direct interpretation of the recorded scenes by means of image content description methods. The novelty of these investigations relies on the fact that the stripe patterns permit at the same time the visual enhancement of the relevant information and a significant reduction of the amount of data to be processed. Such an approach therefore satisfies the major conditions inline inspection systems must fulfill: the robustness in terms of high signal to noise ratio and the low computational costs in order to achieve high inspection throughputs.

The major purposes of this chapter are (i) to give an overview of the actually achieved research results concerning the surface characterization based on the projection and the direct interpretation of structured light patterns, and (ii) to demonstrate that this approach serves the characterization of complex industrial surfaces. The whole quality control process in case of the industrial inspection is addressed. For each main element of the processing chain, a focus on the major achievements is provided: the projection and adaptation of specific stripe patterns (data generation), the segmentation and characterization of these adapted patterns (data processing), and the classification of the corresponding surfaces (data interpretation). This chapter ends by proposing a possible generalization method and gives important further research directions in order to address the inline characterization of complex free-form surfaces.

This chapter is organized into three paragraphs. Paragraph "Data Generation" tackles two possible illumination techniques for the generation of structured patterns. Also the recording of regular patterns in case of complex surface geometries is addressed. The automatic segmentation of disturbed stripe regions is described in paragraph "Data Processing", which also introduces the considered three feature sets for stripe image description. Finally, an application example in case of cylindrical surfaces and its generalization for complex geometries is described in the last paragraph "Data Classification".

In order to consider real-time inline inspection requirements, all the experiments were validated by means of industrial image datasets. Important aspects, such as high robustness against varying recording conditions but also fast data processing for real-time applications are considered.

2. Data generation

The inspection problem is primarily tackled under its optical and physical aspects so that the purpose is to define the optimal data generation in case of structured light based surface inspection. This paragraph is therefore dedicated to the optimization possibilities in case of the generation of optimal stripe structures for the inspection of complex industrial surfaces.

At first, the choice of the appropriate illumination technology is addressed. Two different approaches, a "transmission"-based and "collimation"-based are described and compared. It is demonstrated that the latter is more appropriate for the visual enhancement of geometrical surface deformations on semi-reflective surfaces. The generation of adapted, "inverse patterns", is tackled afterwards. It is demonstrated how far pattern adaptation improves the visual interpretation of geometrical complex surfaces.

2.1 Defining the adequate illumination

2.1.1 Generalities

In the optical inspection domain, the observation of surfaces having different reflection coefficients or various geometries for quality control or metrology purposes is done by means of specific lighting approaches. The key point, and common process for all methods, is to *visually enhance* and characterize the relevant information. The choice of the adequate lighting is task dependent and must be defined according to the surface characteristics (reflectivity, geometry).

Within this context, the use of structured light patterns to reveal geometrical and/or textural surface characteristics has a broad range of applications. While deflectometric approaches (fringe structure projection) are dedicated to specular surface inspection, bright- or dark-field methods (projection of collimated light) can be perfectly suited to matt surface quality control (Abouelela, 2005). However, different techniques to generate such light patterns to be projected exist. We might distinguish between two different light projection approaches, a general one called "transmission", and a more specific one named "collimation". The formalism used here is based on the physical generation principle of the stripe patterns. Each illumination is described in detail, so that the geometrical arrangement and the optical properties of the illumination's main elements are tackled.

2.1.2 The transmission and the collimation approaches

The "transmission" based fringe projection technique is the mostly used and developed within the computer vision community. It can consist in the transmission of diffusing light through a light-transmissive structure or in the transmission of a structured light pattern through a diffusing element. In the last case, structured light patterns can be produced by a LCD (Liquid Crystal Display), a DMD (Digital Micromirror Device), or a DOE (Diffractive Optical Element) device. The principle of the "collimation" is to direct incoming light with, e.g. a 3D fringe selection object (Caulier, 2007), or directional LEDs. Fig. 1 shows the two fringe pattern generation principles with image examples.

Both lighting techniques consist of two different parts: a diffuse illumination and a pattern generation element which filters the light rays using "transmission" or "collimation" techniques. The depicted examples demonstrate that both illuminations lead to similar

fringe structures if similar geometrical deformations on specular surfaces are considered. The case of two different deformations is tackled here: dents (concave) and blisters (convex). Even if the images depict different surfaces, the red bold marked surface regions leading to visible fringe perturbations clearly show the similarity of both lighting techniques, in case of the visual enhancement of geometrical structures.

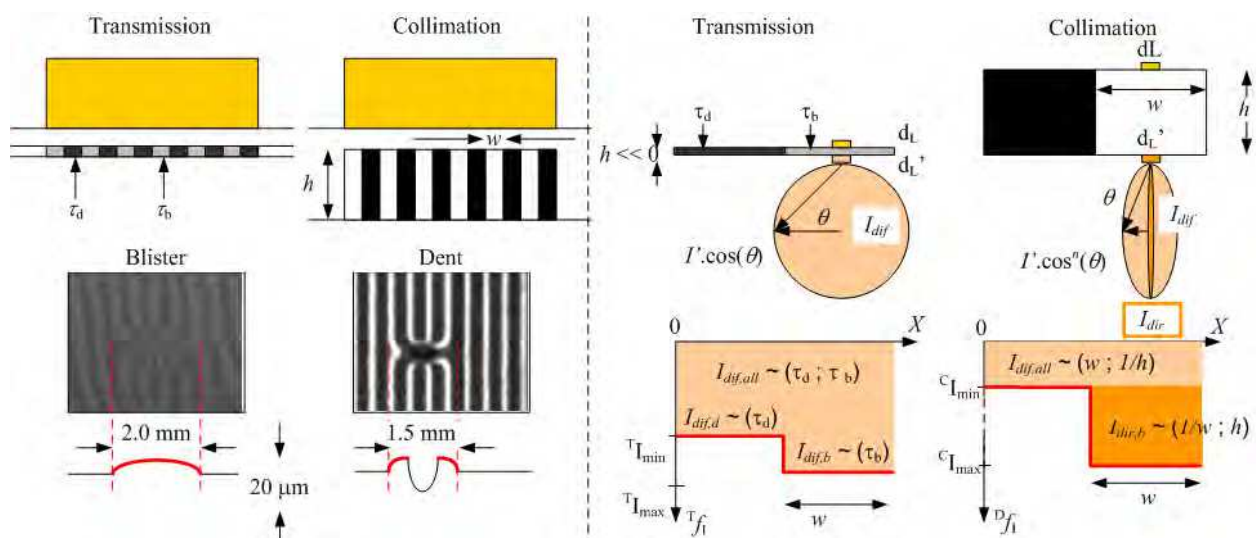


Fig. 1. Principle of the two (i) "transmission" and (ii) "collimation" approaches (left). The theoretical explanation is done for an elementary light source d_L (right). For the transmission technique, the light distribution remains lambertian, whereas for the collimation one, the light intensity profile is more directional. The directionality degree is proportional to the exponent n of the cosine function, where n varies from 0 to infinity. Theoretical intensity profiles T_{f_i} and D_{f_i} for both lightings are depicted.

However, if both illuminations permit similar visual enhancements, the depicted images in Fig. 1 show that the recorded structures are depicted differently, i.e. that the contrast of the light structures is different. The transmission-based lighting seems to produce "smoother" structures than the collimation-based one. This is a fundamental difference which has a direct influence of the processing methods and also on the considered inspection requirements. In the following, both illuminations are theoretically described.

A first simplification hypothesis consists of considering that the diffuse illumination placed before the pattern generation element is an ideal lambertian light source. Thus, the light profile of an elementary illumination element d_L placed *before* the pattern generation can be modeled by a $\cos(\theta)$ function, where θ is the angle between the direction of observation and the normal of d_L . The light profile of an elementary illumination element d_L' *after* the pattern depends of the properties of the structured light filtering element. Light intensity profiles of both models can be expressed with a $\cos^n(\theta)$ function, where n is a factor modeling the light directivity. $n=1$ for the "transmission" approach and $n \geq 1$ for the collimation approach, so that higher values of n are synonymous a higher directivity. If the $\cos^n(\theta)$ function models the shape of the structured light, the light intensity can be modelled by two one-dimensional functions $T_{f_i}(x)$ and $D_{f_i}(x)$, where x is the spatial position along the fringe structure.

These profiles depend on fringe pattern geometrical and physical parameters, which are the transmission factors of bright and dark fringes τ_b and τ_d for the "transmission solution", the

height h , and the fringe width w for both solutions, where $\tau_b > \tau_d$, $\{\tau_b; \tau_d\}$ in $[0:1]$ and $h \ll 1$ for the "transmission" one. Both intensity profiles after fringe light source are obtained by summing for elementary surface $d_L'(x)$ at point x the amount of light coming from all neighboring points on the X-axis. The ${}^T f_I(x)$ and ${}^D f_I(x)$ curves in Fig. 1 vary between two values ${}^k I_{min}$, ${}^k I_{max}$, where k stands for transmission T and directed D . As stated before, the "transmission" lighting consists of a purely diffuse ${}^T I_{dif}$, whereas the "collimation" is made of a diffuse ${}^C I_{dif}$ and a directional ${}^C I_{dir}$ part. ${}^k I_{dif,all}$ is a diffuse part induced by *all* the dark and bright structures, while ${}^k I_{dif,d}$, ${}^k I_{dif,b}$, and ${}^k I_{dir,b}$ are diffuse and directed parts induced by the *considered* dark and bright structures. All these values, and so the bright and dark fringe contrast in the images, depend on the illumination specific parameters τ_b , τ_d , w , h .

One of the important aspects of the projected fringe structure is to optimally visually enhance the relevant surface information, whether for direct interpretation (qualitative) or for reconstruction (quantitative) purposes. Optimal fringe interpretation can be obtained when foreground fringe structure is easily distinguishable, i.e. can be segmented from background object structure. Hence, being able to influence the ${}^k I_{max}$, ${}^k I_{min}$ ratio $R_{b,d}$, but also the ${}^k I_{dif}$ and ${}^k I_{dir}$ ratio ${}^k R_{dif,dir}$ is of major importance. For the theoretical considerations, it can be assumed without loss of generality, that each elementary light source has a diffuse and a directed part. The proportion of each part determines the diffuseness of the directivity of the light source. Thus, the ratios for the "transmission" and "collimation" methods can be expressed as follows (l is a constant and f the light distribution function):

$$\begin{aligned}
 {}^T R_{b,d} &= \frac{I_{dif,b} + I_{dif,all} / 2}{I_{dir,d} + I_{dif,all} / 2} \sim \frac{\tau_b + f(\tau_d; \tau_b) / 2}{\tau_d + f(\tau_d; \tau_b) / 2} \in [1 : l] \\
 {}^T R_{dir,dif}^b &= \frac{0}{I_{dif,all} / 2 + I_{dif,b}} = 0 \\
 {}^C R_{b,d} &= \frac{I_{dir,b} + I_{dif,all} / 2}{I_{dif,all} / 2} \sim 1 + \frac{f(1/w; h)}{f(w; 1/h)} \in [1 : \infty] \\
 {}^C R_{dir,dif}^b &= \frac{I_{dir,b}}{I_{dif,all} / 2} \sim \frac{f(1/w; h)}{f(w; 1/h)} \in [0 : \infty].
 \end{aligned} \tag{1}$$

Major difference of both lightings is that, whereas for the transmission solution, the diffuse part $I_{dif,all}$ is unavoidable, the second solution offers the possibility to have only the directed light component $I_{dir,b}$, i.e. to strongly reduce the diffuse part by increasing the h/w ratio. This is an interesting property, as it permits to increase the visual enhancement of geometrical structures, especially for semi-reflective surface inspection, and decrease the visual appearance of the surface texture.

For surfaces with a non-negligible diffuse reflecting part, geometrical structures are all the more enhanced for high ratios ${}^k R_{b,d}$ and ${}^k R_{dir,dif}$. In case of the "transmission" approach, these ratios are theoretically always l -limited, a theoretically infinite ratio can be obtained with the "collimation" approach. This effect is clearly observable in the corresponding images of Fig. 1 representing a dent-like defect. In case of the "collimation" approach, fringe structures, and so the geometrical surface information, are better visually enhanced, than in case of the "transmission" approach. This is the reason why former approaches are used in case of controlled environments, i.e. when optimal lighting conditions are possible, permitting optimal fringe segmentation, in case e.g. of quantitative 3D reconstruction of matt surfaces.

These results show that in case of geometrical information retrieval, and especially for surfaces with a non-negligible diffuse reflecting part, "collimation" approaches are more appropriate. Values of illumination parameters w and h should be determined in accordance to the inspection requirements, as increasing the ratio h/w decreases the amount of additional diffusing perturbing light $I_{dif,all}$, but also decreases the total amount of projected light $I_{dir,b} + I_{dif,all}$.

2.1.3 The considered illumination technique and reference patterns

As the purpose of this chapter is to propose an alternative surface inspection procedure for the inline characterization of complex objects, a robust methodology based of the projection and interpretation of stripe patterns, will be proposed. These investigations are based in images recorded with an industrial inspection system using a "collimation" illumination, see Fig. 2 Therefore, for the rest of the chapter, the "collimation" lighting will be used. The "transmission-one" will only be considered for theoretical considerations.

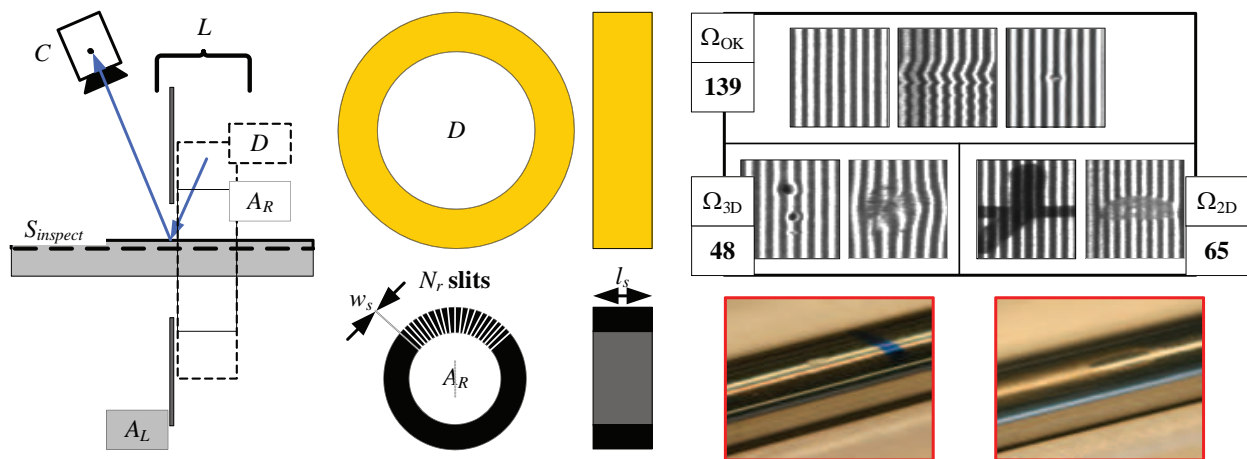


Fig. 2. Considered image datasets (right), recorded with a "collimation" illumination (left), and photos of the cylindrical inspected surfaces (bottom). The illumination L is made of a cylindrical diffusing element D and a slit object A_R to collimation the incoming diffuse light. The line scan camera C records the constant moving surface to be inspected $S_{inspect}$.

Fig. 2 shows some image examples of the considered reference dataset. Each stripe image depicts one type of surface to be characterized, and has been recorded by a special "collimation" illumination producing vertical and periodical stripe structures. The whole set of reference patterns is made of 252 elements manually annotated and classified into three distinct classes Ω_{OK} , Ω_{3D} , and Ω_{2D} . These classes correspond to 139 acceptable surfaces, 48 non-acceptable geometrical defects, and 65 non-acceptable textural defects.

2.2 Generating the appropriate adapted patterns

The second step of the proposed method of this chapter concerns the generation of so called inverse patterns, geometrically adapted to the shape of complex surfaces. Major purpose of this surface inspection methodology, based on the interpretation of regular patterns, is to simplify the processing of the stripe images and therefore to increase the robustness of the proposed approach in case of real-time inline processes. Indeed, as periodical and vertical

bright/dark structures have to be processed, the scene interpretation method is equivalent to a matching operation where an a priori known structure, a regular pattern, is compared with an observed one, the pattern being disturbed by a defective surface. The considered approach, i.e. the recording set-up, the inverse pattern generation principle and the recorded images of complex surfaces, is depicted in Fig. 3.

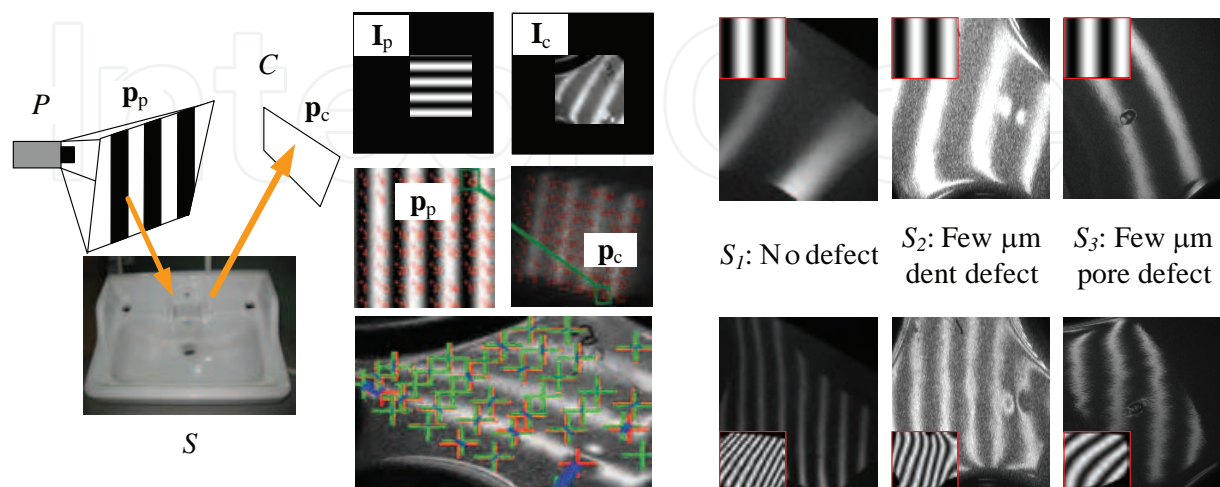


Fig. 3. Considered set-up (left), homography between projector and camera screens (middle) and recorded regular pattern for different complex surfaces (right). The set-up is made of a camera C which records the light structure (i) projected by the projector P and (ii) reflected by the surface to be inspected S . The homography, which permits to link each point p_p of the projector image I_p with a point p_c of the camera image I_c , permits the determination of the adapted patterns, so that vertical and periodical patterns are recorded by the camera.

The provided solution consists of an iterative approach for the determination of the optimal homography linking the projecting screen P and the sensor C recording complex specular surfaces S . Inverse image determination permits the projection of an irregular or "inverse" pattern I_p , so that after its projection on the free-form reflective surface, a regular pattern is depicted in the camera image I_c . For I_c calculation, the following three-step approach was considered in this paper: (i) determination of the position and the size of the structured pattern to be projected, (ii) computation of the screen to camera transformation, and (iii) retrieval of the transformation matrix H , where $I_c = H \times I_p$, permitting the determination of the pattern to be projected. These three steps are addressed in the next paragraphs.

2.2.1 Determining the projector pattern

The size and the position of the structured pattern to be projected have a direct influence on the appearance of the observed structured pattern in the camera image. Thus, pattern position and size in the projector image I_p have to be adapted in order to reduce noisy effects, as double reflection of the structured pattern or the influence of diffuse lighting. Concerning the investigations presented in this paper, these parameters were determined empirically. The point correspondence is then applied to the depicted projector and camera structured patterns.

2.2.2 Iterative matrix transformation determination

Once the correspondence between projector points \mathbf{p}_p and camera points \mathbf{p}_c is determined, the transformation matrix \mathbf{H} linking the two images can be computed. As point correspondence is done in case of free-form surfaces, \mathbf{H} must be modeled by a polynomial equation of degree r , by means of n corresponding reference points, where $n > n_r$, and n_r is the minimum necessary number of points to retrieve the coefficients of polynomial degree r .

The optimization approach here consists of retrieving optimal degree r and number n of points, in order to minimize the value $e_{c,p}$, which is the Residual Mean Square Error (RMSE) of known camera points \mathbf{p}_c and estimated points ${}^{\text{estim}}\mathbf{p}_c$ after applying \mathbf{H} to projector points \mathbf{p}_p . The optimization procedure is described in the following equation:

$$\begin{aligned} H / \bar{e}_{c,p} &= \text{RMSE}(\mathbf{p}_c, {}^{\text{estim}}\mathbf{p}_c), \\ \forall r \in [1 : \infty[, \forall n \in [n_r : n_{ref}[& \end{aligned} \quad (2)$$

where n_{ref} = number of correspondance points.

A two-step procedure is considered here: (i) retrieval of appropriate degree r , its value will depend on the geometrical complexity of the surface ($r = 1$ for the particular case of a planar surface), (ii) determination of optimal number of points n for the transformation. The former serves the determination of the optimal transformation according to the considered free-form surface, the latter permits to consider only robust points, by successively forward selecting the most relevant points. The stopping criterion of forward selection is an a priori defined threshold. An example depicting known points \mathbf{p}_c (green), estimated points ${}^{\text{estim}}\mathbf{p}_c$ (red) and error $e_{c,p}$ (blue) is depicted in Fig. 3.

2.2.3 Surface characterization with computed patterns

The evaluation of the method is done visually. For this, three different free-form surfaces with different geometrical complexity are considered. The depicted images in Fig. 3 show how surface visual enhancement is improved by means of the proposed “inverse pattern” method. A geometrical defect is depicted on two of these three surfaces, S_2 and S_3 . These results are comparable to the detection of sub-millimeter depths defects using the 3D surface reconstruction with the shape from specular reflection technique, see (Balzer, 2010).

The proposed method permits to project an adapted pattern, so that a regular vertical pattern can be observed in the camera image. As discussed previously, pattern regularity will depend on different parameters, where the geometrical surface complexity is the most determinant.

These results show that the appearance of the regular patterns generated with a “transmission” lighting is similar to the patterns generated by a “collimation” one, see the reference dataset depicted in Fig. 2. This is the reason why, the next paragraphs dedicated to the data processing and classification will tackle the interpretation of the “collimation” patterns. The similarity between both types of patterns will also permit to generalize the results to the automatic inspection of complex surfaces.

3. Data processing

The second part of this chapter involves specific signal and image processing methods. The investigations are focused on multiresolution approaches in the frequency and in the spatial domains. The aim is to retrieve the relevant information from the recorded stripe data, i.e. to segment the perturbed stripe structures synonymous of defective surfaces and to characterize the selected regions by means of appropriate feature-based approaches. These two aspects are tackled in the next paragraphs.

3.1 Free-form segmenting stripe image regions

Once the scene to be characterized has been visually enhanced, the next step consists of the characterization of the stripe regions synonymous of defective surfaces. As the purpose of the characterization is to describe the image regions depicting disturbed stripes, these image parts must be preliminary segmented before being described via feature-based approaches.

The segmentation of stripe structures, so that only the disturbed stripe structure to be characterized is depicted in the pattern, has been addressed in previous researches. It has been demonstrated that for some image content analysis approaches, the segmented images leads to higher classification rates than the images with fixed square sizes (Caulier, 2010). However, hand-segmenting each image region before its classification is, of course, not possible in terms of a fully automatical inspection process, so that unsupervised and adapted segmentation procedures should be defined. Such automatic processes are very often linked with segmentation errors (Unnikrishnan, 2007).

Conventional segmentation processes can be coarsely divided into *contour-based* approaches consisting of determining the transitions between image regions, and *region-based* approaches whose principle is to group image points together with similar characteristics. Although these techniques have been extensively described in the literature, we did not find yet some automatic segmentation approaches of stripe structures. This is in fact a rather complex task, as the depicted defective surfaces by means of stripe patterns are usually not characterized by sharp contours, as these are overlaid by the projected bright/dark stripes. A “simple” solution would be to segment the image patterns to classify by means of sliding overlapping windows of constant sizes. The magnitude of the overlapping regions should be defined according to the specifications of the inspection task.

However, the considered stripe segmentation methodology in this chapter uses an innovative multiscale (wavelet-based) technique permitting the segmentation of free-form relevant image regions. The proposed method, originally developed for the automatic detection of visual saliencies, relies on the assumption that the regions to be detected correspond to denser energy distributions at different scales and frequency subbands. As visual saliencies methods mimic the human visual perception, these are also part of bio-inspired approaches.

3.1.1 The bio-inspired approach

The principle of the bottom-up visual attention model attempts to predict which location in the image will automatically and unconsciously attract the observer’s attention towards them. In this biologically-inspired system, an input image is decomposed into a set of

multiscale neural "feature maps" which extract local spatial discontinuities in the modalities of color, intensity and orientation. Each feature map is endowed with non-linear spatially competitive dynamics, so that the response of a neuron at a given location in a map is modulated by the activity in neighboring neurons. Such contextual modulation, also inspired from recent neurobiological findings, has proven remarkably efficient at extracting salient targets from cluttered backgrounds. All feature maps are then combined into a unique scalar "saliency map" which encodes for the salience of a location in the scene irrespectively of the particular feature which detected this location as conspicuous. Fig. 4 depicts the considered model of (Itti, 1998).

3.1.2 Stripe segmentation based on visual saliency map

Concerning the bio-inspired stripe structure segmentation, following reasoning is made. Visual saliency algorithms permit to sample in detail the most relevant features of a scene, i.e. the scene parts containing most important image information. Thus, it is assumed, that in case of the addressed stripe segmentation problematic in this paper, the image parts to be segmented also correspond to the parts with high visual saliency, so that a biological approach can be used as a preliminary segmentation step.

For the purposes of this chapter, we will consider the approach of Itti and Koch (Itti, 1998), encompassing a feature map generation, a center-surround computation, and an across-scale combination until final saliency map generation. The considered method is an image to image transformation, where input data is the stripe structured scene to be segmented and characterized, and output data is the saliency representation of the input scene, which corresponds to high attention degree. Fig. 4 shows the computed saliency maps by means of the considered ITTI approach (Itti, 1998) for three different scene examples belonging to the three considered classes Ω_{OK} , Ω_{3D} , Ω_{2D} .

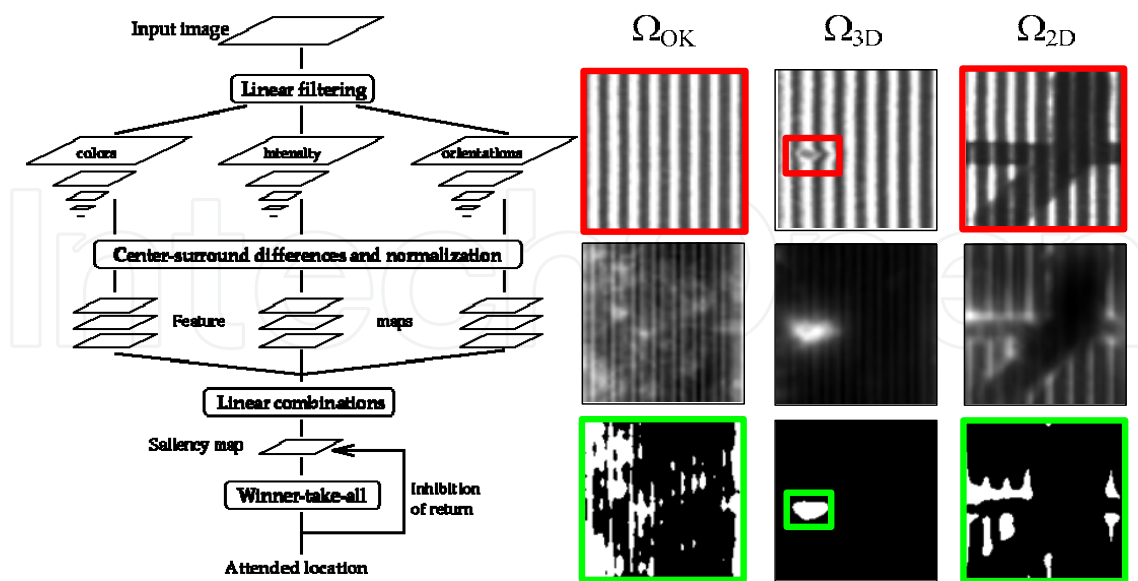


Fig. 4. Considered bio-inspired approach of Itti (Itti, 1998) and examples of saliency maps for three different surface types. The red rectangles correspond to the image regions to be automatically segmented. The green rectangles are the selected regions after binarization of the saliency maps.

The Fig. 4 shows how saliency maps permit to reveal certain stripe structures. If the image contains a salient region, i.e. a locally disturbed pattern, the values of this saliency map region are higher than the surrounding ones. Otherwise, if the pattern remains homogeneous, i.e. corresponds to a non defective surface, no particular image region is revealed by the map. In case of the depicted images, the grey values of the saliency map are higher on the defective regions in case of the Ω_{3D} and the Ω_{2D} images, whereas grey values are more homogeneous for the Ω_{OK} image. A simple binarization of the maps followed shows how far the ITTI approach permits a good object/background differentiation, in particular for locally disturbed patterns. In the following we will see how these saliency representations can be used for the segmentation of stripe patterns.

Saliency maps give a spatial representation the saillancies in an image: the higher the values of a map, the higher the probability that the region (object) differ from the surrounding pixels (background). These maps can therefore be seen as the results of a testing procedure, as the grey value of a pixel map $I_s(i,j)$ is proportional to the probability $P(O)$ that this pixel belongs to a region to be classified. Thus, the discrimination between object and background classes, Ω_{object} and $\Omega_{\text{background}}$, is equivalent to a classification procedure consisting of the determination of a binarization threshold γ . All pixel whose grey values are higher than γ are classified as object region, whereas all other as background region. This can be stated as follows:

$$\begin{aligned} &\text{if } I_s(i,j) > \gamma \text{ then } I_s(i,j) \in \Omega_{\text{Object}} \text{ else } I_s(i,j) \in \Omega_{\text{Background}} \\ &\forall (i,j) \in [n_l, n_c] \\ &\text{where } [n_l, n_c] \text{ is the size of the image } I_s(i,j) \text{ and } \gamma \in [0, 255]. \end{aligned} \quad (3)$$

However, a global binarization procedure also implies falsely classified pixels. The fundamental problem therefore consists of determining the most optimal threshold γ_{optim} , so that most of the image pixels are correctly classified into the classes Ω_{object} and $\Omega_{\text{background}}$. For the following we will consider the classification error rate p_{error} of [Zha01], who permits to evaluate the segmentation process of a map I_s for a certain threshold γ and the previously described reference image database.

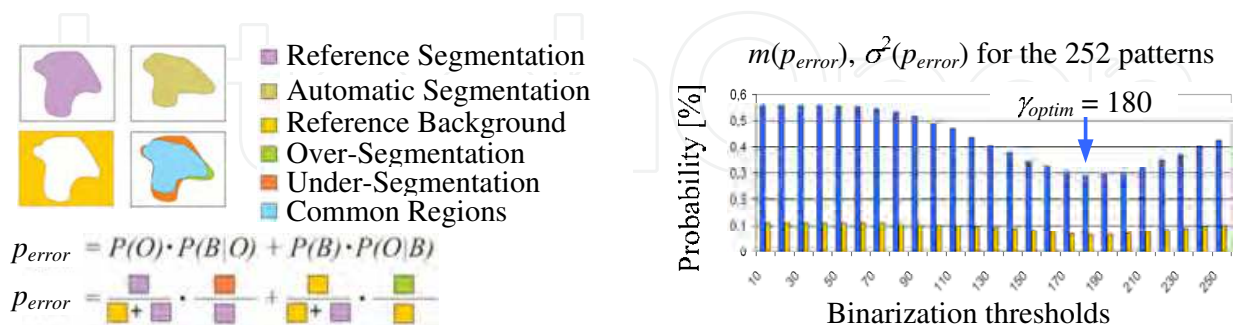


Fig. 5. Computation principle of p_{error} (left) and curves $m(p_{\text{error}}), \sigma^2(p_{\text{error}})$ permitting the determination of γ_{optim} (right).

The consider approach for determining the optimal threshold γ_{optim} consists of computing the error rate p_{error} for all threshold values $[0,255]$, so that optimal threshold will correspond to the lower rates p_{error} . In order to define one threshold for the segmentation of all possible

stripe images, the mean $m(p_{error})$ and the variance $\sigma^2(p_{error})$ for the error rates for all 252 images of the reference dataset will be used to evaluate each threshold γ . Fig. 5 depicts show the computation principle of p_{error} and the computed values of $m(p_{error})$ and $\sigma^2(p_{error})$ for the 252 stripe images.

The two curves represent the evolution of $m(p_{error})$ and $\sigma^2(p_{error})$, computed with the considered dataset of 252 stripe images, for each threshold γ . It is noticeable how both curves reach a minimum for the same value of $\gamma_{optim} = 180$. This value, which corresponds to the lowest classification error rate, is the optimal threshold values γ_{optim} .

3.2 Characterization of stripe image regions

Once the regions of interest, i.e. these depicted non-acceptable surface parts, have been segmented, these can be characterized in a second step by means of feature-based approaches. Preliminary investigations showed that optimal stripe characterizations are achieved using adapted and Fourier features. New multiresolution features are introduced in this paragraph. Spatial transformations using Gabor filters are considered. In the following all the considered feature sets are introduced.

3.2.1 The feature based image characterization principle

According to Randen and Husoy (Randen, 1999), it is a-priori not possible to know which textural method is more appropriate for a specific task. A selection of the most appropriate one (methods partially based on work by Wagner and Kueblbeck (Wagner, 1996) and Wagner (Wagner, 1999) was done. Most publications dedicated to *specific* features-based stripe structure characterization are related to fringe pattern identification within the field of interferometric non-destructive inspection. Type and number of described fringe features are task dependent. We may distinguish between spatial-based (Jueptner, 1994; Zhi, 1992), frequency-based (Takeda, 1982; Qian, 2005), and mixed (wavelet) (Krueger, 2001; Li, 2000) approaches.

The selected methods for the addressed problems in this chapter correlate with the highest recognition rates of the described methods and studies: (i) the *transform* of Weska, (ii) the adapted of Zhi (Zhi, 1992), and (iii) the multiresolution of Mallat (Mallat, 1989). As few publications tackle the problems of image structure characterization, a particular attention was given to the retrieval of specific adapted features. For our purposes, *four geometry* and *two statistic-based features* proposed by (Zhi, 1992) for bright stripe pattern characterization were applied. The contribution to specular surface inspection is achieved through the completion of these features with additional *four specific features*. The novel aspect consists of the use of these features for the characterization of the bright stripes, but also of the dark stripes within the pattern.

These methods being part of general approaches belonging to the main texture families (Tuceryan, 1998) or of specific methods, specially developed for the characterization of image structures. Each of these procedures was optimized by adapting method innate parameters towards the depicted disturbed or non-disturbed stripe pattern (shape, intensity e.g.).

Fig. 6 shows the computation principle for the first two considered features sets, the Fourier and the Stripe ones.

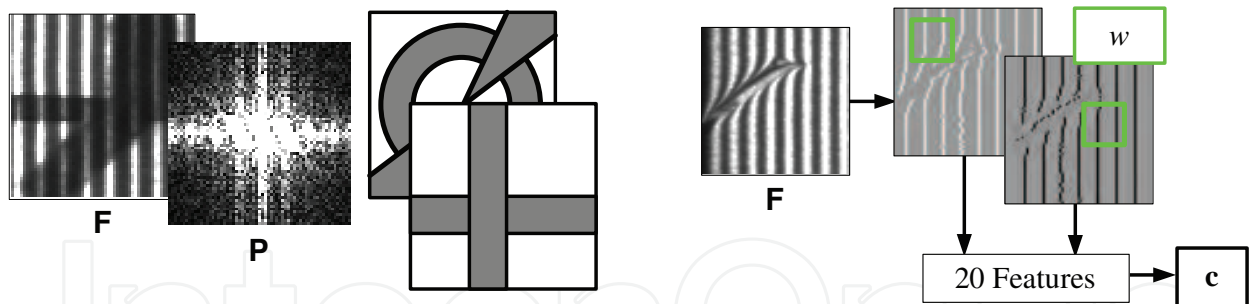


Fig. 6. Computation principle of the Fourier (left) and the Stripe (right) feature sets. The Fourier features correspond to the spectral energy of different regions of the Fourier spectrum. The figure shows the original image F , its power spectrum P and horizontal, vertical, directional and radial energy regions. The stripe features correspond to the intensity- and geometry-based description of the segmented bright and dark stripe structures. Each feature is first locally computed for different image pixels using a window w . The final feature value for an image F is the average of all the locally computed feature values.

3.2.1.1 Fourier textural features

The DFT (Discrete Fourier Transform) made the spectral analysis of discrete images possible, by decomposing the image function into a sum of finite sinusoids. The textural transform approach proposed by Weska (Weszka, 1978) is based on the spectral domain analysis. The features are computed from values in the Fourier spectrum corresponding to different r_F radial and d_θ directional spectral regions. As the characterized stripes have a vertical and periodical structure, further u_F and v_F spectral regions along the u -horizontal and the v -vertical image axes were defined.

The vector computation for the involved Fourier textural analysis method is depicted below:

$$C_{r,\theta,v,h}^F = \{C_r^F; C_\theta^F; C_v^F; C_h^F\}, N_c = 33 (= 8 + 10 + 5 + 10) \quad (4)$$

3.2.1.2 Adapted fringe and stripes features

The considered bottom-up approach is based on preliminary investigations (Caulier, 2008) involving specific geometry-based and intensity-based features according to a two-step procedure, stripe *segmentation* and *characterization*. Each process is characterized by following parameters: the segmentation function f utilized and the image areas a that are covered by a local window w sliding over the entire pattern described. Notation for the sub-pixel segmentation peak detectors are b^5 for the "Blais-and-Rioux" and c^5 for the "Center-of-Mass", see (Caulier, 2008). Hence notations for considered segmentation functions are $f \in \{b^5; c^5\}$. Concerning the characterization of the extracted bright and dark regions each feature $c_{a(m)}^S$ represents the average result of an $O_{a(m)}(m)$ operation applied to a bright or dark stripe element. The computation of $O_{a(m)}(m)$ is applied to an image area $a(m)$, whose magnitude is feature dependent.

The new contributions consist of applying the features 9 to 14 defined in (Caulier, 2008) for the bright stripes, also to the dark stripes, so that a total of 20 features are considered here, m

$\in \{0, \dots, 19\}$. Hence, from these 20 features, 8 were specially developed for the considered stripe images, whereas the 12 remaining were described within the context of fringe structure characterization (Zhi, 1992) and adapted for our purposes. It is these 8 features which were used in the industrial application (Caulier, 2008). The description of the stripe feature vector with the different area magnitudes $a(m)$ is as follows:

$$C_{f,a}^S : f \in \{f_b; f_c\} \text{ and } a = [a(0), \dots, a(m), \dots, a(19)],$$

$$a(m) \in \left\{ [5^2]; [7^2]; \dots; [17^2]; [M_u \times M_u] \right\}, N_c = 20 \quad (5)$$

The maximal value of $a(m)$ is determined according to the minimal possible size of the reference stripe patterns which is approximately 20 pixels. As mentioned above, the computation of the stripe feature vector relies on two segmentation functions f . Then, each of the stripe feature vector's 20 elements can be computed by means of 8 different area sizes of $a(m)$. Hence, 2×8^{20} stripe feature vectors can be retrieved based on the definition provided in Equation 5. In order to reduce the number of possible feature stripe vectors, and thereby avoiding dimensionality-based problems, a preliminary optimization process to retrieve the most adequate area size of $a(m)$ for each feature $c_{a(m)}^S$ is necessary.

When considering the definitions of the 20 operators, we can distinguish between the features whose computation relies on *fixed* and *adapted* image areas $a(m)$, where m is the feature index. For fixed areas, the only condition is that the area sizes must be large enough to allow both operators to be applied. For adapted image areas, the most appropriate area size must be defined according to the stripe structures to be characterized.

Preliminary studies (Caulier, 2008) show that an optimal set of image areas \mathbf{a}^1 , depicted in following Equation, can be defined (maximum possible area size is noted $M^2 = [M_u \times M_v]$):

$$\mathbf{a}^1 : \{ \{a(00) - a(05); a(08) - a(09)\} = [M^2]; \dots$$

$$\dots \{a(06) - a(07); a(10) - a(15); a(18) - a(19)\} = [17^2]; \quad (6)$$

$$\dots \{a(16) - a(17)\} = [5^2] \}$$

In order to validate the tests described in (Caulier, 2008), an additional "non-optimal" set \mathbf{a}^2 , complementary of \mathbf{a}^1 , i.e. $M^2 = [M_u \times M_v]$ value remains, 5^2 and 17^2 values must be exchanged, was also considered.

3.2.2 Proposed Gabor wavelet features

Generalities

Major drawback of the Fourier approach, is that if it permits a good spatial resolution, it is not possible in the same time to have a good resolution in the frequency domain, this phenomena is known as the Heisenberg inequality or uncertainty principle. The purpose is here to investigate how far a multiresolution approach can be used for the classification of stripe image patterns. The considered procedure consists of using the approach of Mallat (Mallat, 1989) and to systematize it to another other wavelet family. The Gabor one will be

used. For the Fourier approach, the directional regions of the power spectrum lead to best discrimination results, see paragraph 5.2.1. Hence, using a wavelet decomposition approach, the influence of the combined selection of different frequency regions with the selection of different decomposition levels will be investigated.

For each level, the wavelet coefficients are obtained by convolutions of input image $f(u,v)$ with two one-dimensional filters: h a lowpass filter and g a highpass filter, with $g(n) = (-1)^{1-n} h(1-n)$. A detailed procedure of the image wavelet decomposition can be found in (Mallat, 1989). Fig. 7 describes the wavelet decomposition and reconstruction principle at level r of an image signal $f(u,v)$ with a pyramidal representation according to Mallat (Mallat, 1989).

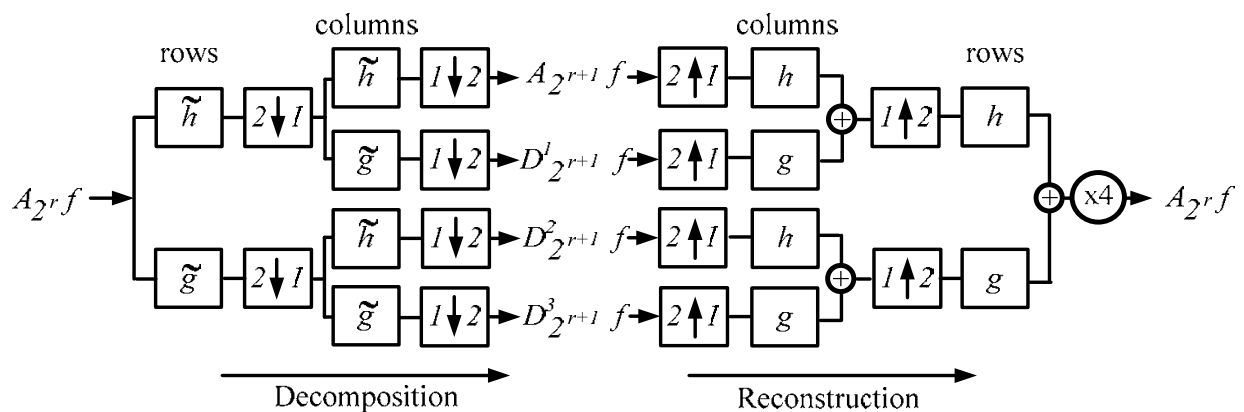


Fig. 7. Decomposition and reconstruction principle of the discrete wavelets transform in the spatial domain according to (Mallat, 1989).

Classification methodology with wavelets

First classification step consists of wavelet decomposing each image. The energy measure of the four subband images $A_{2^r} f$, $D_{2^r}^1 f$, $D_{2^r}^2 f$ and $D_{2^r}^3 f$ for each decomposition level r is used as signature for each image. Unlike the Fourier transform, which just utilizes the sine and cosine as basis functions, each new wavelet family brings its own set of new basis functions (the necessary conditions such functions must fulfill are defined in (Mallat, 1989) Section III.A).

As the purpose is to evaluate the classification of stripe image patterns using different types of textural features, the activities are focused on one wavelet family, the Gabor wavelet filters (Kovesi, 2011). This approach was considered to be an appropriate enhancing function, as these filters permit the enhancement of image structures of different shapes, frequencies and orientations. In the following a brief overview of 2D Gabor is provided.

According to the definition of Dunn (Dunn, 1995) which is based on the definition of Daugman (Daugman, 1985), a 2D Gabor filter h is an oriented complex sinusoidal wave h_{sin} modulated by a 2D Gaussian envelope h_{gau} , $h = h_{sin} \times h_{gau}$. Filter main parameters are the wavelength $\lambda = 1/f$, f is the frequency, the standard deviation σ and the orientation α .

Different values of these parameters permit the elaboration of different filters of different shapes, sizes and directions.

For the purpose of this chapter, the Gabor filter definition given by Kovési will be considered. The author defines three output images, I_r , I_i , I_a , results of the convolution of the input image I_{in} with the (i) real part h_r of the 2D filter h , the (ii) imaginary part h_i of the 2D filter h and the (iii) amplitude of both real and imaginary images. Filter description according to Kovési (Kovési, 2011) for the x -direction is provided by the following equation (for the sake of simplicity, the x -direction was considered, same equations hold for the y -direction by replacing the x with y):

$$f_r = \cos\left(\frac{2\pi}{\lambda} \chi \cdot\right) \cdot e^{-\left(\frac{x^2}{\sigma_x^2}\right)} \cdot f_\alpha \quad f_i = \sin\left(\frac{2\pi}{\lambda} \chi \cdot\right) e^{-\left(\frac{x^2}{\sigma_x^2}\right)} \cdot f_\alpha$$

where $\sigma_x = \lambda \cdot k_x$ (7)

$$I_r = I_{in} * f_r \quad I_i = I_{in} * f_i \quad I_a^2 = I_r^2 + I_i^2$$

f_α is a rotating function defined for an angle α in degrees (an angle of 0 gives a filter that responds to vertical features. The scale factors k_x and the filter σ_x relative to the wavelength of the filter. This is done so that the shapes of the filters are invariant to the scale. k_x controls the shape of the filter in the x -direction.

According to equation 7, λ permits to regulate the modulation of the \cos and \sin waves with the Gaussian envelope. For $\lambda=1$ the filtering is equivalent to an image blurring with a Gaussian kernel, and therefore reveals low image frequencies. Higher values of λ and of k permit image filtering with Gaussian kernel modulated with \cos or \sin envelopes, which is equivalent to convolve the image with second or first derivative filter kernels. Thus, in case of high image frequencies enhancement and if the edge information is considered as important images signatures, a variation of the variance σ of the Gaussian kernel between $\sigma \in [2:4]$ seems to be an adequate choice.

Therefore, for the purposes of this chapter, the Gabor filterbank is made of Gabor filter values, $l = 2$ and $k=2$, so that $\sigma= 4$, two orientations, $\alpha = 0^\circ$ and $\alpha = 90^\circ$. The \sin function was considered. These filters were applied for the computation of image features. Four decomposition levels $r = \{ 2, 3, 4, 5 \}$, corresponding to object sizes in the image of $\{ 4, 8, 16, 32 \}$ were considered. Hence, the resolution given by the considered stripe structure which is $d_{p,px}=8$ pixels is taken into consideration, see the images in Fig. 2. It is assumed that the resolution level $r=3$ could bring interesting classification results.

Classification methodology with wavelets simple decomposition

This first classification procedure uses all computed approximation and detail images during Mallat's decomposition algorithm using the Gabor wavelet. First element of Wavelet's simple decomposition feature vector c_{ws} equals the energy value of original image F . Then, the remaining elements of c_{ws} are filled with the energy values of the approximated and all detail images obtained by decomposing the image F . Following expression of feature vector $c_{ws} \in R^{N_c}$ is obtained by decomposing image F until level r with Gabor wavelet:

$$\begin{aligned}
c_{WS} &= \{E(0, f), E(1, A), E(j, D^1), E(j, D^2), E(j, D^3)\}, \\
c_{WS} &\in R^{N_c}, \quad N_c = 2 + 3r \\
\text{with } j &= \{1, \dots, r\}, \quad r \in Z
\end{aligned} \tag{8}$$

Where $E(0, f)$ is the energy of original image pattern F .

Classification with wavelets generalized decomposition

A shortcoming of the conventional dyadic wavelet transform is that it does not benefit from possibly useful features that can be obtained by further decomposing the high frequency subbands. An improvement therefore consists of decomposing also the high frequencies (Coifman, 1992; Tikkanen; 1997, Nasir, 2002; Cohen1997) i.e. in computing the approximation and detail images not only for the approximation image $A_{2^{r+1}}f$ at each level r but also for the detail images $D_{2^{r+1}}^1 f$, $D_{2^{r+1}}^2 f$, and $D_{2^{r+1}}^3 f$ ($r > 1, r \in Z$). This general wavelet decomposition approach will be named the *generalized multiresolution decomposition* also named wavelet packet analysis (Tikkanen, 1997).

A feature vector \mathbf{c} is made of the energy values of all approximation and detail images computed during the generalized multiresolution decomposition. First element of \mathbf{c} equals the energy value of original image F . Following expression feature vectors of Wavelet's generalized decomposition is obtained:

$$\begin{aligned}
c_{WG} &= \left(E(0, f), \{E(j, k, A)\}, \{E(j, k, D^1)\}, \{E(j, k, D^2)\}, \{E(j, k, D^3)\} \right) \\
c_{WG} &\in R^{N_c}, N_c = 1 + \sum_{j=0}^r 4^j \\
\text{with } j &= \{1, \dots, r\}, \quad k = \{1, \dots, 4^j\} \quad r \in Z
\end{aligned} \tag{9}$$

Where $E(0, f)$ is the energy of the original image pattern F and $E(j, k, A)$, $E(j, k, D^1)$, $E(j, k, D^2)$, $E(j, k, D^3)$ are the energies at level j of the subband image numbers k .

Classification with subband wavelet generalized decomposition

This further investigation consists of the evaluation of each subband separately, in order to figure out how far the selection of a particular subband can lead to an improvement of the reached classification rates. For this purpose the images are classified each by means of the four subband images obtained with a generalized wavelet decomposition approach. In order to really estimate which of the four coefficients contain the most discriminating information, we consider the *generalized* wavelet decomposition for the decomposition level $r=3$, as this level correspond to the size of the considered period of the reference images, which is $2^3 = 8$.

Doing this, four feature vectors are defined. $\mathbf{c}_{SWG, (D2,3,A)}$ contains the energy of all approximation images $A_{2^{r+1}}f$ up to level $r=3$ using Gabor wavelet and the *generalized* Wavelet decomposition. Feature vectors $\mathbf{c}_{SWG, (3,A)}$, $\mathbf{c}_{SWG, (3,D1)}$, $\mathbf{c}_{SWG, (3,D2)}$ and $\mathbf{c}_{SWG, (3,D3)}$ are filled with the energy of all detail images $D_{2^{r+1}}^1 f$, $D_{2^{r+1}}^2 f$, and $D_{2^{r+1}}^3 f$ up to level $r=3$ using

Gabor wavelet and the *generalized* Wavelet decomposition. Following expressions of feature vector using the Wavelet's subband generalized decomposition are obtained:

$$\begin{aligned}
 c_{SWG,(3,A)} &= \left(\{E(j,k,A)\} \right) \in R^{N_c} \\
 c_{SWG,(3,D^1)} &= \left(\{E(j,k,D^1)\} \right) \in R^{N_c} \\
 c_{SWG,(3,D^2)} &= \left(\{E(j,k,D^2)\} \right) \in R^{N_c} \\
 c_{SWG,(3,D^3)} &= \left(\{E(j,k,D^3)\} \right) \in R^{N_c}
 \end{aligned} \tag{10}$$

$$N_c = \sum_{j=1}^r 4^{j-1}$$

with $j = \{1, \dots, r\}, \quad k = \{1, \dots, 4^{j-1}\} \quad r \in Z$

Where $E(j,k,A)$, $E(j,k,D^1)$, $E(j,k,D^2)$, $E(j,k,D^3)$ are the energies at level j of the subband image numbers k .

4. Data interpretation

The third and last part of this chapter is dedicated to the interpretation, i.e. classification, of the generated metadata by means of data mining techniques. The general purpose is to retrieve, for a specific inspection task, the optimal processing chain, i.e. leading to high detection and low false alarm rates. The proposed procedure uses a classification factor as an evaluation criterion for the direct evaluation and comparison of different data processing approaches.

It is demonstrated that this procedure can be applied for the evaluation of any image processing tasks. In a first step, the method is validated for a certain surface shape within the context of a specific inspection purpose. In a second step, the case of complex free-form structure characterization is used for the generalization of the method. The considered reference stripe image dataset was introduced at the beginning of this chapter in paragraph 3.1.3.

4.1 Optimal processing chain determination

As described at the beginning of this chapter, the purpose is to demonstrate how the projection of adapted structured patterns can be used for the inline inspection of complex reflective surfaces. Within the context of industrial non destructive testing, an inspection system has been developed for the characterization of cylindrical specular surfaces (Caulier, 2009). The principle relies on the combination of a collimation-based illumination and line scanning cameras to record and process the reflected regular patterns. Fig. 2 shows some images examples depicting defective cylindrical surface parts.

The system's requirements are automatically to classify the surfaces of the recorded cylindrical objects into non-defective, defective geometrical or defective textural. This three-class problem consists of determining the most optimal processing chain based on the

feature-based description of the recorded stripe image. The aims are here (i) to determine most appropriate stripe segmentation approach, (ii) to evaluate the relevance of the proposed feature sets, (iii) to retrieve the most optimal one, and (iv) to generalize the approach and the results obtained with the inspection of cylindrical surfaces to the interpretation of complex surfaces.

The problem is therefore tackled in two steps. At first, the lowest complexity problem of most appropriated processing chain retrieval within the context of regular stripe characterization is addressed. For this, in order to retrieve the most appropriate feature set, the previously described Fourier and Stripe features are evaluated by means of three different *image sets*, three different *classifiers*, and one *classification methodology*. Thus, for each of the four feature sets, *nine* different pattern analysis procedures were considered.

Then, the generalization is done by using the most optimal features defined for the characterization of “simple” surface for the interpretation of complex objects. As the aim is also to retrieve the most appropriate feature sets, here also different processing chains will be evaluated. However, as the purpose is the generalization to complex surfaces, the investigations will be focused on (i) the compare of *nine* different image sets taken reference databases, and on (ii) the involving of special feature subset selection (FSS) methods based on the previously defined optimal classifier.

4.2 Optimal processing chain for cylindrical surfaces

As defined previously, concerning the *image sets*, three segmentation approaches were considered: (i) a free-form approach as described in the paragraph 4.1, *image sets* Φ_{ff} , and (ii) fixed sizes of 64x64 pixels and 128x128 pixels, with *image sets* Φ_{64^2} , Φ_{128^2} . The patterns were recorded with the industrial system (Cau2007c), see the examples in Fig. 2.

In order to address a general stripe pattern characterization approach, the proposed empirical method involved three different classification principles, all using a specific technique or a particular configuration. Following classifiers were involved: The non-parametric Nearest-Neighbor approach, **1-NN** for $k=1$, **3-NN** for $k=3$, and, the parametric Naive Bayes **NB**, applied to the previously cited classifiers. As to the *classification methodology*, and a stratified 10-fold cross validation (Kohavi, 1995), were chosen.

All the results are shown in Tables 1 and 2. These tables list the stripe patterns' (i) classification using Fourier's, the Stripe's and the Gabor wavelet's features.

Different generalities can be done concerning the segmentation process, the classification approach and of course the feature sets, on the basis of the results listed in both tables.

At first, free-form segmentation approaches seem to be more appropriated for Wavelet and Stripe features. The common aspect of both approaches is to use the average results of spatial filters applied to the reference images for feature vector construction. Free-form segmentation permits to retrieve only the disturbed parts of the whole stripe structures to be characterized, and to discard the undisturbed ones in case of defective surface characterization, and contrariwise to retain only the undisturbed part in case of non defective surface characterization, see Fig. 4. In other word, free-form segmentation permits a first spatial discrimination between disturbed and undisturbed stripe regions. The assumption is therefore that, such segmentation techniques are more appropriate to classification methods using spatial filters for feature vector computation.

	Fourier vectors	Image sets			Stripe vectors	Image sets		
		Φ_{ff}	Φ_{64^2}	Φ_{128^2}		Φ_{ff}	Φ_{64^2}	Φ_{128^2}
NB	c_F	63,4	75,4	61,5	$c_{SISC,g1,BR5}$	84,9	84,5	78,3
	$c_{F,(r)}$	58,3	67,2	57,8	$c_{SISC,g1,CM5}$	83,7	82,8	60,0
	$c_{F,(\theta)}$	66,4	80,4	55,8	$c_{SISC,g2,BR5}$	79,6	75,8	61,4
	$c_{F,(v)}$	49,2	79,3	58,8	$c_{SISC,g2,CM5}$	77,6	73,8	57,1
	$c_{F,(u)}$	54,8	41,0	36,2				
1-NN	c_F	79,2	84,9	84,4	$c_{SISC,g1,BR5}$	88,1	85,3	8,2
	$c_{F,(r)}$	72,7	69,8	65,7	$c_{SISC,g1,CM5}$	88,9	81,6	82,8
	$c_{F,(\theta)}$	78,2	87,9	83,6	$c_{SISC,g2,BR5}$	86,1	85,9	83,5
	$c_{F,(v)}$	76,9	79,2	75,9	$c_{SISC,g2,CM5}$	84,6	78,4	78,8
	$c_{F,(u)}$	65,0	75,6	61,5				
3-NN	c_F	76,2	58,3	81,3	$c_{SISC,g1,BR5}$	86,5	84,3	80,5
	$c_{F,(r)}$	68,6	70,6	65,8	$c_{SISC,g1,CM5}$	84,5	77,7	80,9
	$c_{F,(\theta)}$	75,8	81,2	82,5	$c_{SISC,g2,BR5}$	83,5	81,7	81,1
	$c_{F,(v)}$	74,3	77,8	75,7	$c_{SISC,g2,CM5}$	82,2	78,8	74,8
	$c_{F,(u)}$	63,9	75,6	64,7				

Table 1. Rates of correctly classified patterns of the three image sets Φ_{ff} , Φ_{64^2} , Φ_{128^2} for the Fourier and the adapted Stripe features.

	Vector	Image sets				Image sets				Image sets		
		Φ_{ff}	Φ_{64^2}	Φ_{128^2}		Φ_{ff}	Φ_{64^2}	Φ_{128^2}		Φ_{ff}	Φ_{64^2}	Φ_{128^2}
NB	$c_{W,S,(D2,2)}$	53,7	53,7	51,1	$c_{W,G,(D2,2)}$	58,1	56,4	52,1	$c_{SW,G,(D2,3,A)}$	64,9	59,2	48,5
	$c_{W,S,(D2,3)}$	78,5	71,2	63,1	$c_{W,G,(D2,3)}$	64,2	58,2	51,6	$c_{SW,G,(D2,3,D1)}$	78,3	75,4	66,0
	$c_{W,S,(D2,4)}$	83,9	80,3	77,4	$c_{W,G,(D2,4)}$	65,1	61,8	75,4	$c_{SW,G,(D2,4,D2)}$	60,0	58,6	55,1
	$c_{W,S,(D2,5)}$	86,5	83,2	61,8	$c_{W,G,(D2,5)}$	70,1	64,5	57,3	$c_{SW,G,(D2,5,D3)}$	85,7	77,3	71,2
1-NN	$c_{W,S,(D2,2)}$	74,1	71,6	73,9	$c_{W,G,(D2,2)}$	72,0	71,4	71,6	$c_{SW,G,(D2,3,A)}$	76,4	75,2	70,2
	$c_{W,S,(D2,3)}$	82,6	79,2	75,2	$c_{W,G,(D2,3)}$	84,2	82,8	75,2	$c_{SW,G,(D2,3,D1)}$	78,7	75,5	66,3
	$c_{W,S,(D2,4)}$	76,5	74,5	74,0	$c_{W,G,(D2,4)}$	83,0	82,1	78,4	$c_{SW,G,(D2,4,D2)}$	80,9	81,6	81,4
	$c_{W,S,(D2,5)}$	76,0	76,2	75,2	$c_{W,G,(D2,5)}$	81,0	81,6	79,4	$c_{SW,G,(D2,5,D3)}$	82,3	79,4	72,6
3-NN	$c_{W,S,(D2,2)}$	70,4	72,4	69,5	$c_{W,G,(D2,2)}$	78,6	74,5	68,7	$c_{SW,G,(D2,3,A)}$	78,4	76,1	68,4
	$c_{W,S,(D2,3)}$	75,0	75,0	75,5	$c_{W,G,(D2,3)}$	80,1	76,4	72,0	$c_{SW,G,(D2,3,D1)}$	79,3	75,5	68,5
	$c_{W,S,(D2,4)}$	80,1	76,0	77,6	$c_{W,G,(D2,4)}$	83,7	81,2	78,8	$c_{SW,G,(D2,4,D2)}$	81,9	81,7	81,4
	$c_{W,S,(D2,5)}$	75,4	75,4	74,8	$c_{W,G,(D2,5)}$	81,2	79,2	76,9	$c_{SW,G,(D2,5,D3)}$	82,4	82,0	74,6

Table 2. Rates of correctly classified patterns of the three image sets Φ_{ff} , Φ_{64^2} , Φ_{128^2} for the Gabor Wavelet features.

Concerning the use of adapted images, we remark that better classification rates are reached for fixed image sizes, and especially for the Φ_{64^2} image set. In fact, the Fourier spectrum is applied to images whose sizes equal a power of two, so that in case of variable image sizes a padding with zeros is necessary. Hence, as far as Fourier features are concerned, the image region containing the stripe to be characterized but also the surrounding image region contains important discriminative information.

Then concerning the classifiers, Tables 1 and 2 show that in general best classification rates were obtained using the 1-NN classifier for the three considered feature types. For the Wavelet features, the most appropriate classifiers depend on the involved feature vector computation techniques. For the Fourier features, we remark that optimal results were reached for the reduced feature set $c_{F,(\theta)}$ involving only the ten directionality power spectrum features. For this configuration, the classification rates are similar to those obtained with the whole 33 features and even better.

To conclude, it is observable that wavelet features do not seem to be the more appropriate in case of the considered classification task, i.e. in comparison with the Fourier and the Stripe techniques. Classification rates with Wavelet features are the lowest and no particular classifier seems to be more appropriate, as for each of the three considered wavelet feature computation techniques, a different classifier leads to highest classification rates.

4.3 Generalization to complex surfaces

4.3.1 Generalization of the reference image dataset

The generalization concerns the projection of adapted patterns in order to observe regular patterns, which can be characterized with the previously described methodology. Major advantage of the adapted pattern projection method, compared to similar 3D reconstruction ones, see (Ihrke, 2008; Balzer, 2010), is to visually enhance geometrical defects on complex free-form surfaces, for the purpose of qualitative direct surface characterization.

However, in case of inline inspection systems perturbing effects leading to non optimal surface characterization by means of adapted projected pattern interpretation may occur. Major perturbing factors are due to imperfect recording conditions or surface characteristics. In case of workpiece positioning above the defined moving tolerances e.g., additional noise such as defocusing or light glares, will perturb the reference point determination. Also in case of small surfaces, whose size does not permit to project enough stripe patterns, the point determination might not be optimal. In addition, certain surfaces, such as e.g. several layered light transmitting ones, may also lead to sub-optimal visual appearance of the stripe in the recording sensor.

This signifies that in case of a generalization of the proposed surface characterization method based on the projection of stripe patterns, the reference dataset must be enlarged in order to cover all possible regular patterns to be characterized.

The task is not to enumerate all possible regular stripe pattern disturbances. This would hardly be possible. Hence, it is preferable to focus our investigations on a restricted and predefined number of *not perfectly vertical* and *not perfectly periodical* stripe patterns.

Further pattern structures have therefore to be defined. The easiest and simplest way consists of using the considered set introduced in paragraph 4.2 and to "transform" or "adapt" them, so that these can be used for the characterization of free-form surfaces.

Thus, the stripe-illumination-based complex surface inspection task will be addressed by means of different image sets: The reference initial set Φ_0^0 previously introduced, and eight further derived sets. The four sets Φ_1^1 - Φ_1^4 correspond to the warping of all patterns of Φ_1^1 with increasing projective transformations. The four sets Φ_2^1 - Φ_2^4 correspond to the warping of all patterns of Φ_0^0 with increasing cylindrical transformations. Two projective -1- and cylindrical -2- transformations have been considered. All sets are made of 252 patterns.

Fig. 8 shows 3 of the 9 considered stripe image data sets. Φ_0^0 is the reference set where the stripe structures are periodical and vertical, Φ_1^4 is the set corresponding to the warped patterns of set Φ_0^0 with a maximum perspective distortion -1- and Φ_2^4 is the set corresponding to the warped patterns of set Φ_0^0 with a maximum cylindrical distortion -2-.

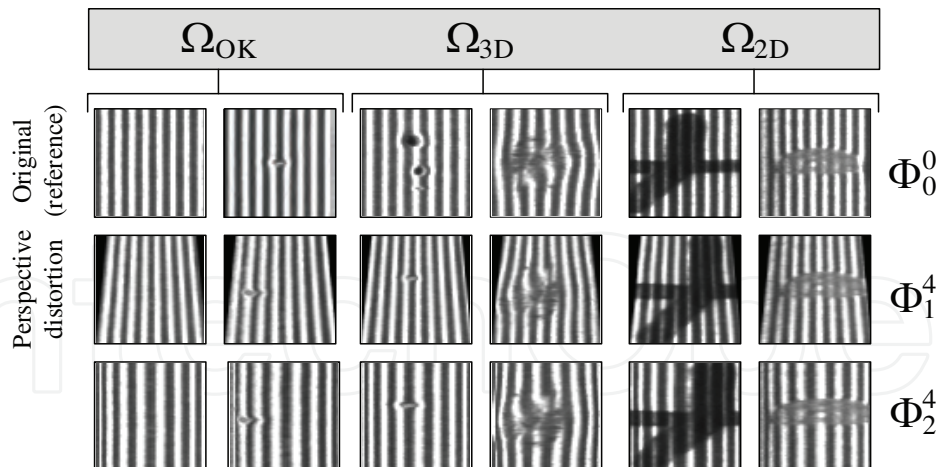


Fig. 8. Reference patterns for the classification of free-form rough and specular surfaces. The figure shows 6 image examples taken from the three different pattern sets Φ_0^0 , Φ_1^4 and Φ_2^4 .

These image patterns correspond to three different complex surfaces illuminated with an adapted pattern: -0- for surfaces ideally depicted, and -1- and -2- for surfaces inducing perspective and cylindrical distortions.

Φ_1^4 and Φ_2^4 corresponds to patterns with a maximal perturbation of type -1- and a maximal perturbation of type -2-. These patterns have been simulated by transforming patterns Φ_0^0 [The first number is an indices the second is an exponent] with perspective and cylindrical distortions. All the patterns have a size of 64 x 64 pixel.

4.3.2 Optimal processing chain for increased surface complexity

This paragraph addresses the procedure for the determination of optimal feature subsets using feature evaluation, grouping, fusing, and selection in case of the general inspection problem stated in this paper, i.e. the inspection of complex objects using structured illumination. It has been demonstrated in the previous paragraph 4 that two feature families, the 33 Fourier and the 20 adapted stripe features, lead to best classification rates. In order to define to appropriate features sets in case of the generalization to complex surfaces, feature subset selection (FSS) methods are evaluated by considering the generalized reference databases.

The question is to what extend an appropriate fusion and selection of the Fourier and the adapted stripe feature sets can lead to a better quality control of the complex surfaces? For this purpose, two group of three feature vectors will be considered. First group consists of vectors $\mathbf{c}_{r,\theta,v,u}^F$, made of the 33 Fourier features, \mathbf{c}_{θ}^F , made of the 10 directional Fourier features, and \mathbf{c}^S consisting of the 20 adapted features. Second group encompasses vectors $\mathbf{c}_{r,\theta,v,u}^{F,S}$, made of the 33 Fourier features and the 20 adapted stripe features, $\mathbf{c}_{\theta}^{F,S}$ made of the 10 directional Fourier features and the 20 adapted stripe features, and ${}^{1\text{-NN}}\mathbf{c}_{\theta}^{F,S}$ made of the selected features of vector $\mathbf{c}_{\theta}^{F,S}$ using a 1-NN-wrapper-based FSS method. Classification results using the three two feature vector groups and the two distortion types are depicted in Fig. 9.

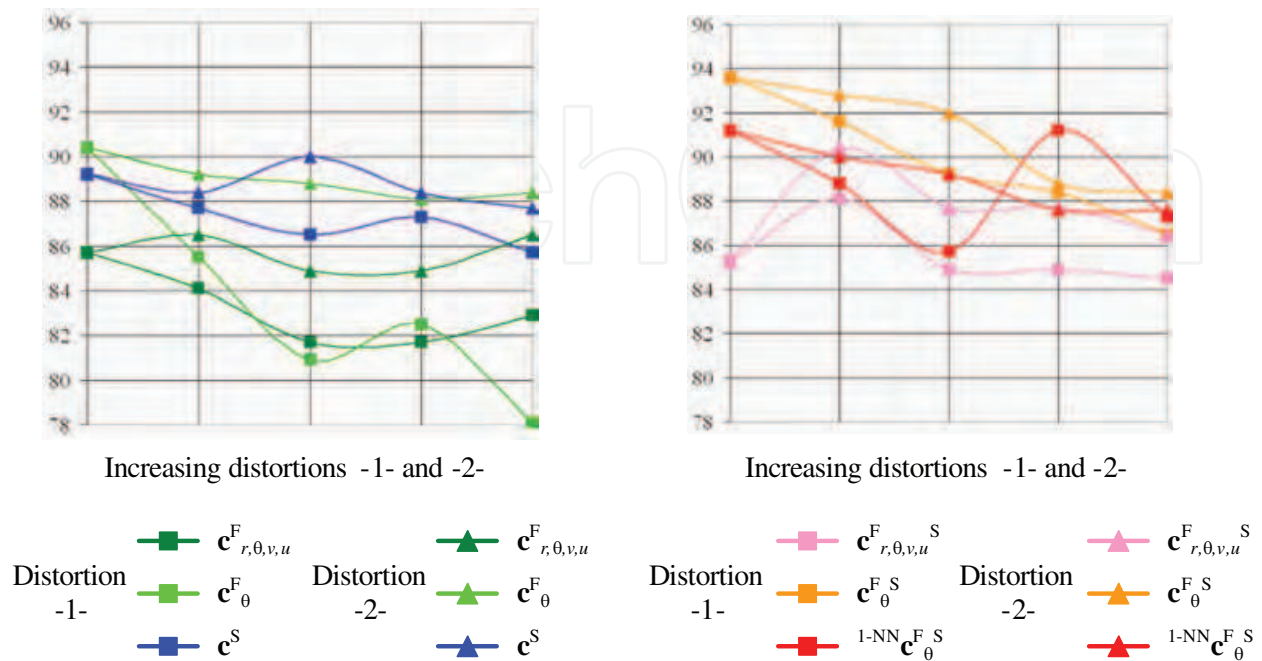


Fig. 9. Classification rates for image distortions of type -1- and of type -2- by means of the two groups of feature vectors $\{ c^F_{r,\theta,v,u}; c^F_\theta; c^S \}$ and $\{ c^F_{r,\theta,v,u}^S; c^F_\theta^S; 1\text{-NN } c^F_\theta^S \}$.

The detection rates were computed for different image sets and correspond to increasing distortions of type -1- and of type -2-. Left to right values: detection rates for image set Φ_0^0 to image sets Φ_1^4 and Φ_1^2 . On the whole, the reported classification rates in Fig. 9 (right) are higher than those depicted in Fig. 9 (left). This shows the importance of determining the adequate features with the appropriate feature selection processes. In case of the considered inspection task, optimal features sets are 10 directional Fourier features and the 20 adapted stripes feature, whereas the optimal feature selection method is the wrapper-based 1-NN approach. However, if the feature fusion permits to reach higher classification rates of approximately 2 % (difference between the maximal detection rates of both considered graphics), the FSS method does not improve the classification rates, as similar or even lower classification results are observed when the FSS method is applied.

The last investigation is dedicated to a more detailed depiction of the considered FSS method, in order to determine the relevant features.

4.3.3 Optimal features in case of the generalization approach

In order to determine the most relevant features the influence of increasing distortions of type -1- and of type -2- on the number and types of selected features is investigated. Table 3 shows the results in case of a wrapper 1-NN approach and a 10-fold cross-validation.

Feature set	Type -1- distortion					Type -2- distortion				
	Φ_0^0	Φ_1^4	Φ_2^4	Φ_3^4	Φ_4^4	Φ_0^0	Φ_1^4	Φ_2^4	Φ_3^4	Φ_4^4
$N_{c,sub}$	90	90	95	107	108	90	99	107	116	107
$c^S(00)$	0	0	0	0	0	0	0	1	0	0
$c^S(01)$	1	1	0	0	3	1	1	0	1	0
$c^S(02)$	0	0	0	0	0	0	0	2	0	0
$c^S(03)$	0	0	1	2	3	0	0	3	2	3
$c^S(04)$	3	3	2	8*	2	3	3	4	5	3
$c^S(05)$	4	4	1	3	3	4	2	1	3	5
$c^S(06)$	2	2	4	1	0	2	4	1	5	8*
$c^S(07)$	9**	9**	3	8*	3	9**	8*	7	6	5
$c^S(08)$	6	6	6	3	3	6	6	6	6	6
$c^S(09)$	7	7	4	6	4	7	5	4	4	2
$c^S(10)$	7	7	6	7	5	7	4	6	6	1
$c^S(11)$	0	0	3	5	4	0	0	1	1	0
$c^S(12)$	6	6	3	3	5	6	6	2	6	1
$c^S(13)$	2	2	6	8*	10***	2	5	5	8*	4
$c^S(14)$	0	0	1	0	7	0	4	4	4	3
$c^S(15)$	0	0	3	2	7	0	5	0	2	6
$c^S(16)$	9**	9**	6	6	9**	9**	4	6	3	4
$c^S(17)$	2	2	5	10***	6	2	1	4	5	8*
$c^S(18)$	1	1	5	4	6	1	3	0	4	6
$c^S(19)$	6	6	8*	10***	9**	6	7	7	7	4
$c^F_\theta(0)$	0	0	2	1	0	0	0	0	0	1
$c^F_\theta(1)$	0	0	2	1	1	0	1	3	3	2
$c^F_\theta(2)$	5	5	3	4	1	5	7	4	5	5
$c^F_\theta(3)$	4	4	5	2	3	4	2	5	2	3
$c^F_\theta(4)$	4	4	4	1	3	4	5	9	6	6
$c^F_\theta(5)$	10***	10***	10***	10***	10***	10***	10***	10***	10***	10***
$c^F_\theta(6)$	0	0	0	1	0	0	2	4	0	0
$c^F_\theta(7)$	1	1	2	1	0	1	2	2	5	4
$c^F_\theta(8)$	1	1	0	0	1	1	1	5	3	1
$c^F_\theta(9)$	0	0	0	0	0	0	1	1	4	6

Table 3. Selected features when a wrapper 1-NN approach is used for increasing distortion of type -1- and -2-. The maximum number of times a feature can be selected is 10. The variables $N_{c,sub}$ on the left give the total number of selected features after the 10 runs. The 10 time, 9 time and 8 time selected features are marked with ***, ** and *. Results for all relevant features are marked in bold.

An important parameter is the variable $N_{c,sub}$, which is the total number of selected features after the 10 runs of the 10-fold cross-validation. As 10 is the maximum number of times a feature can be selected, $N_{c,sub} / 10$ is the average measure of feature relevance. For both tables, increasing the distortion of the bright/dark structures, leads to an increase of the necessary relevant features.

A general remark for both tables concerns the types and the number of selected features, which are approximately the same. It appears that approximately seven features, i.e. only a fourth of the initial 30 ones, are relevant. Most of the selected features are adapted ones, whereas mainly the directional 90° Fourier features have a strong relevance.

It is also noticeable, that feature relevance is related to the bright/dark structure distortion degree. As an example, in case of both tables, the importance of feature $c^s(13)$ is proportional to the distortion degree, whereas the contrary is observed for feature $c^s(07)$.

5. Conclusion

The chapter addressed the inspection by means of structure lighting of complex surfaces within the context of industrial inline quality control processes. The whole processing chain was considered by first tackling the structured light generation, then the processing of the acquired images, and finally the classification of the segmented and characterized structured light patterns.

At first, the generation of appropriate structured light patterns has been tackled. From the two described illumination techniques, the “transmission” and the “collimation” one, it has been demonstrated that the latter is more appropriate for the characterization of geometrical structures as such a lighting technology permits to reduce the diffuse part of the reflected light. As the aim of the chapter is to define a general approach for complex surface interpretation by means of structured lighting, a general and adapted method has been presented. The principle consists of recording and processing regular patterns by projecting patterns which are adapted to the complex geometries of the surfaces under inspection. The generation of adapted patterns uses coded light to determine the homography linking the screen and camera points for pattern adaptation. Different images examples validate the proposed procedure.

The second part was dedicated to the adapted segmentation of the generated structured patterns. The originality of the proposed method relies on the use of a bio-inspired approach to compute saliency maps. It has been showed how such maps permit to reveal disturbed regions of stripe patterns synonymous of defective surface parts. The proposed free-form segmentation procedure consists of a saliency map generation preceding a binarization. It has been showed how a supervised approach permits to compute the most optimal threshold for all the considered reference images. The segmented stripe patterns were characterized afterwards by means of different features, whose innate parameters were adapted to the special task of stripe pattern interpretation. Two features sets lead to highest classification rates, the Fourier and the adapted Stripe features.

The third and last part addressed the definition of the most optimal stripe structures processing chain by using the classification rate as evaluation criteria. The purpose is to tackle the inspection of complex surfaces. At first, a reference industrial inspection system using a “collimation” lighting for generating regular patterns, has been considered. By means of the classification rate, it has been demonstrated that the most optimal chain consists of (i) defining 64×64 pixels fixed size patterns, (ii) processing them with Fourier and adapted Stripe features, and (iii) classifying the computed vector with a 1-NN classifier.

In a second part, the general inspection task consisting of interpreting complex surface has been tackled. The most optimal processing chain for complex surface interpretation was defined (i) by generalizing the reference dataset to more complex surfaces and (ii) by retrieving the adapted feature sets using a wrapper-based selection feature procedure. The results showed that only a certain number of features are relevant, and that reduced but appropriate features permit to reach classification rates for complex surfaces similar to rates obtained with more "simple" geometries.

To conclude, this chapter proposed a feature-based surface characterization methodology based on the direct interpretation of regular patterns, adapted to the geometrical complexity of the surface. This approach permits to reach higher positioning tolerances in case of real-time surface inspection. As no depth information is computed, the proposed inspection procedure is more dedicated to binary decisions, i.e. whether the surface is defective or not. However, such detailed characterization is not necessary in case of the real-time industrial surface inspection. A preliminary determination of the projected pattern characteristics in accordance to the smallest critical defects to be detected is sufficient in this context.

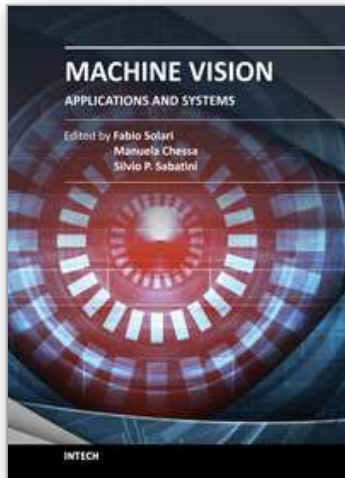
6. References

- Abouelela, A., Hazem M. and Eldeeb, H. and Wahdan, A. and Nassar, S. M.. (2005). Automated vision system for localizing structural defects in textile fabrics. *Pattern Recognition Letters*, Vol. 26, No. 10, pp. 1435-1443.
- Balzer, J.; Werling, S. (2010). Principles of Shape from specular reflections. *International Journal of Measurement*. Vol. 43, No. 10. pp. 1305-1317.
- Caulier, Y.; Spinnler, K.; Bourennane, S.; Wittenberg T.. (2007) New structured Illumination Technique for the Inspection of High Reflective Surfaces. *EURASIP Journal on Image and Video Processing*.
- Caulier, Y.; Spinnler, K.; Bourennane, S.; Wittenberg T.. (2008). Specific Features for the Analysis of Fringe Images. *Optical Engineering Journal*, Vol. 47, No. 5. pp. 057201-01-057201-11.
- Caulier, Y. Andreas Goldschmidt, Spinnler, K.; Arnold, M. Automatic detection of surface and structural defects on reflecting workpieces. *Photonik international*. Vol. 2.
- Caulier, Y.; Bourennane, S.. Visually Inspecting Reflective Surfaces: A Feature-Based Approach. (2010). *Transactions on Pattern Analysis and Machine Intelligence (TPAMI)*, 2010.
- Cohen, A.; Daubechies, I.; Feauveau, J.-C. (1997). Biorthogonal bases of compactly supported wavelets. *Communications on Pure and Applied Mathematics*. Vol. 45, No. 5, pp. 485-560.
- Coifman, R. and Meyer, Y. and Wickerhauser, V. (1992). Wavelet analysis and Signal Processing, In: *Wavelets and their applications*. Ruskai, M. B., pp. 53-178, Jones and Bartlett Publishers, 978-0867202250.
- Daugman, J.. (1985). Uncertainty relation for resolution in space, spatial frequency and orientation optimized by two-dimensional visual cortical filter. *Optical Society of America*. Vol. 2, pp. 1160-1169.

- Dunn, D. (1995). Optimal Gabor Filters for Texture Segmentation. *IEEE Trans. in Image Processing*. Vol. 7., No. 4, pp. 947-964.
- Ihrke, I. and Kutulakos, K. N. and Lensch, H. P. A. and Magnor, M. and Heidrich, W.. (2008). State of the Art in Transparent and Specular Object Reconstruction. *EUROGRAPHICS 2008 STAR - State of the art report*, 2008.
- Itti, L.; Koch, C.; Niebur, E.. (1998) A model of saliency-based visual attention for rapid scene analysis. *IEEE Transactions on Pattern Analysis and Machine Intelligence*, Vol. 20, No. 11, pp. 1254-1259.
- Jüptner, W. and Kreis, T. and Mieth, Ulrike and Osten, Wolfgang. (1994). Application of neural networks and knowledge-based systems for automatic identification of fault-indicating fringe patterns. *Proceedings of SPIE, Photomechanics*. Warsaw, Poland, May, 1994.
- Kohavi, R.. A Study of Cross-Validation and Bootstrap for Accuracy Estimation and Model Selection. *Proceedings of Proceedings of the 14th international joint conference on Artificial intelligence*, 1-55860-363-8, San Francisco, 1995.
- Kovesi, P. D. (2011). MATLAB and Octave Functions for Computer Vision and Image Processing. In: *Centre for Exploration Targeting, School of Earth and Environment*, Available from: <http://www.csse.uwa.edu.au/~pk/Research/MatlabFns>.
- Krüger, S.; Wernicke, G.; Osten W.; Kayser, D.; Demoli, N.; Gruber, H.. (2001) Fault detection and feature analysis in interferometric fringe patterns by the application of wavelet filters in convolution processors. *Journal of Electronic Imaging*, Vol. 10, No. 1, pp. 228-233.
- Li, X.. (2000). Wavelet transform for detection of partial fringe patterns induced by defects in nondestructive testing of holographic interferometry and electronic speckle pattern interferometry. *Optical Engineering Journal*. Vol. 39, No. 10, pp. 2821.
- Mallat S.. (1989). A Theory for Multiresolution Signal Decomposition: The wavelet Representation. *IEEE Transaction of Pattern Anal. and Machine Intell.*, Vol. 11, No. 7, pp. 674-693.
- Rajpoot, N. M.. Texture Classification Using Discriminant Wavelet Packets Subbands. *Proceedings of the 2002 45th Midwest Symposium on Circuits and Systems*, 0-7803-7523-8, 4-7. August 2002.
- Qian, K.; Seah, H. S.; Asundi, A. (2005). Fault detection by interferometric fringe pattern analysis using windowed Fourier transform. *Measurement Science and Technology*, Vol. 15, pp 1582-1587.
- Randen, T.; Husoy, J. H.. (1999). Filtering for Texture Classification: A Comparative Study. *IEEE Transactions on Pattern Analysis and Machine Intelligence*, Vol. 21, No. 4, pp. 291-310.
- Takeda, M.; Ina, H.; Kobayashi, S.. (1982). Fourier-transform method of fringe-pattern analysis for computer-based topography and interferometry. *Journal. Optical. Society of America*. Vol. 72, No. 1, pp. 156-160.
- Tikkanen, P. E.; Sellin, L. C.. Wavelet and Wavelet Packet Decomposition of RR and RT max interval time series, *Proceedings of the 19th Annual International Conference of the IEEE Engineering in Medicine and Biology Society*, 0-7803-4262-3, Chicago, IL., USA, 30 October-2 November 1997.

- Tuceryan, M.; Jain, A.. (1998). Texture Analysis, In: *The Handbook of Pattern Recognition and Computer Vision (2nd Edition)*, Chen, C. H.; Pau, L. F.; Wang, P. S. P., pp. 207-248.
- Unnikrishnan, R.; Pantofaru, C.; Hebert, M.. (2007). Toward Objective Evaluation of Image Segmentation Algorithms. *IEEE Transaction of Pattern Anal. and Machine Intell.*, Vol. 29, No. 6, pp. 929-944.
- Wagner, T.; Kueblbeck, C.. (1996). Automatic Configuration of Systems for Surface Inspection. *Machine Vision Application in Industrial Inspection*, Vol. 3029, No. 1, pp. 128-138.
- Weszka, J.. (1978). A survey of threshold selection techniques. *Journal of Computer Graphics and Image Processing*. Vol. 7, No. 2, pp. 259-265.
- Wagner, T.. (1999). Automatische Konfiguration von Bildverarbeitungssysteme. University of Erlangen-Nürnberg, Germany.
- [Zha01] A review of recent evaluation methods for image segmentation. Technical report, Department of Electronic Engineering, Tsinghua University, Beijing, China, 2001.
- Zhi, H.; Johansson, R. B. (1992). Interpretation and Classification of Fringe Patterns, *Proceedings of 11th International Conference on Image, Speech and Signal Analysis*, 0-8186-2920-7, The Hague, Netherlands, 30 August-3 September 1992.

IntechOpen



Machine Vision - Applications and Systems

Edited by Dr. Fabio Solari

ISBN 978-953-51-0373-8

Hard cover, 272 pages

Publisher InTech

Published online 23, March, 2012

Published in print edition March, 2012

Vision plays a fundamental role for living beings by allowing them to interact with the environment in an effective and efficient way. The ultimate goal of Machine Vision is to endow artificial systems with adequate capabilities to cope with not a priori predetermined situations. To this end, we have to take into account the computing constraints of the hosting architectures and the specifications of the tasks to be accomplished, to continuously adapt and optimize the visual processing techniques. Nevertheless, by exploiting the low-cost computational power of off-the-shelf computing devices, Machine Vision is not limited any more to industrial environments, where situations and tasks are simplified and very specific, but it is now pervasive to support system solutions of everyday life problems.

How to reference

In order to correctly reference this scholarly work, feel free to copy and paste the following:

Yannick Caulier (2012). Characterization of Complex Industrial Surfaces with Specific Structured Patterns, Machine Vision - Applications and Systems, Dr. Fabio Solari (Ed.), ISBN: 978-953-51-0373-8, InTech, Available from: <http://www.intechopen.com/books/machine-vision-applications-and-systems/characterization-of-complex-industrial-surfaces-with-specific-structured-patterns>

INTECH
open science | open minds

InTech Europe

University Campus STeP Ri
Slavka Krautzeka 83/A
51000 Rijeka, Croatia
Phone: +385 (51) 770 447
Fax: +385 (51) 686 166
www.intechopen.com

InTech China

Unit 405, Office Block, Hotel Equatorial Shanghai
No.65, Yan An Road (West), Shanghai, 200040, China
中国上海市延安西路65号上海国际贵都大饭店办公楼405单元
Phone: +86-21-62489820
Fax: +86-21-62489821

© 2012 The Author(s). Licensee IntechOpen. This is an open access article distributed under the terms of the [Creative Commons Attribution 3.0 License](#), which permits unrestricted use, distribution, and reproduction in any medium, provided the original work is properly cited.

IntechOpen

IntechOpen